Journal of Imaging Science and Technology® 51(6): 473–485, 2007.

Spectral Gamut Mapping using LabPQR

Shohei Tsutsumi▲
Imaging Technology Development Center, Canon Inc., 30-2, Shimomaruko 3-Chome, Ohta-ku, Tokyo 146-8501, Japan
E-mail: tsutsumi.shohei@canon.co.jp

Mitchell R. Rosen▲ **and Roy S. Berns**▲
Munsell Color Science Laboratory, Chester F. Carlson Center for Imaging Science, Rochester Institute of Technology, 54 Lomb Memorial Drive, Rochester, New York 14623-5604

Abstract. *Spectral color management requires inversion of printer spectral characterizations and necessarily involves the concept of spectral gamut mapping. A printer was spectrally characterized and the spectra were transformed to an interim connection space (ICS), a spectral description space with low dimensionality useful for building lookup tables (LUTs) of feasible sizes. LabPQR is the ICS used. It has separate dimensions describing colorimetry (CIELAB) and a spectrum's metameric black difference from a standard metamer (PQR). The relationship between digital value and LabPQR was inverted using a single stage objective function combining colorimetric and spectral criteria. The objective function's colorimetric criterion minimized CIEDE2000 under chosen conditions and its spectral criterion minimized Euclidian distance in PQR coordinates. A weight series was performed to find the optimal trade-off between colorimetric and spectral error. A 1:50 weighting ratio, CIEDE2000 to PQR difference, was deemed best. For the GretagMacbeth ColorChecker, the proposed single stage objective function showed equivalent levels of the performance to a full 31-dimensional unmodified spectra approach, resulting in an average RMS error of 4.18% and an average CIEDE2000 of 0.03. The single stage objective function for spectral gamut mapping using LabPQR proved to be promising for spectral reproduction. © 2007 Society for Imaging Science and Technology.*
[DOI: 10.2352/J.ImagingSci.Technol.(2007)51:6(473)]

INTRODUCTION

An important goal of spectral color management is to reproduce images that match originals under arbitrary illuminants. Spectral reproduction requires new approaches including spectral profiling of devices, spectral profile connection spaces, spectral image processing, and new quality metrics. Spectral color management will take advantage of all these concepts and require transformation chains that deliver high-quality results quickly. The spectral characterization of a printer[1–3] yields the forward relationship from fractional area coverage to spectra. An inversion of the printer characterization is necessary so fractional area coverages can be chosen for a requested spectrum. Spectral gamut mapping[4–6] is necessary when considering the problem of spectral color management because an answer must be delivered for any arbitrary spectral request. Unfortunately, spectra typically comprise 31 or more dimensional values. For the purposes of spectral color management, Rosen and co-workers have proposed that spectra be converted to a lower-dimensional interim connection space (ICS).[7–10]

Derhak and Rosen proposed an ICS called LabPQR.[4–6] LabPQR is a six-dimensional ICS that has three colorimetric axes (CIELAB) plus additional spectral reconstruction axes (PQR). PQR describes a stimulus' metameric black,[11,12] a spectral difference between the metameric and the standard spectra. Thus, the PQR coordinates represent the spectral difference between original and reconstructed spectra from colorimetric values.

Rosen and Derhak compared several gamut mapping techniques in PQR and discovered that the approach minimizing PQR difference resulted in lower spectral error.[5] Intuitively, since PQR describes a stimulus' metameric black, Rosen and Derhak's results seem reasonable. However, there was no mathematical explanation that the PQR difference had correlation with the spectral error. Also, Rosen and Derhak evaluated their proposed approaches only in PQR coordinates. There has been no study that tried to evaluate the gamut mapping techniques in the full six-dimensional LabPQR space.

Accordingly, this research explored the feasibility of spectral gamut mapping using LabPQR. First, an appropriate spectra-to-LabPQR transform was built, comparing reconstruction accuracies for unknown spectra. Then, for the spectral gamut mapping, an objective function was defined to perform the colorimetric and spectral matchings in a single stage. In this stage, the spectral characterization of a six-color ink jet printer is inverted. This approach is necessary for building lookup tables (LUTs) for use in spectral color management.

THEORY

LabPQR

LabPQR[4–6] is a six-dimensional ICS. The first three dimensions are CIELAB values under a specific viewing condition, and the additional dimensions are spectral reconstruction dimensions describing a metameric black (PQR),[11,12] as stated above. The metameric black is a spectral difference between the metameric and standard spectra. The PQR co-

▲IS&T Member

Received Nov. 27, 2006; accepted for publication May 7, 2007.
1062-3701/2007/51(6)/473/13/$20.00.

ordinates represent the spectral difference between original and reconstructed spectra from colorimetric values. A six-dimensional example of LabPQR has been discussed in the literature[4–6] and it has been demonstrated for use in spectral gamut mapping.[5,13]

Spectral reconstruction from six-dimensional LabPQR is as follows:

$$\hat{\mathbf{R}} = \mathbf{T}\mathbf{N}_c + \mathbf{V}\mathbf{N}_p, \tag{1}$$

where $\mathbf{T}$ is a n by 3 transformation matrix, $\mathbf{V}$ is a n by 3 matrix describing PQR bases, $\mathbf{N}_c$ is a tristimulus vector, $\mathbf{N}_p$ is a vector of PQR values, and n counts wavelength. Note that $\mathbf{T}$ is applied to tristimulus values converted from CIELAB values. Using a set of the tristimulus vectors, the transformation matrix $\mathbf{T}$ is determined by a matrix calculation using least square analysis[14,15]:

$$\mathbf{T} = \mathbf{R}\mathbf{N}_c^{\mathrm{T}}(\mathbf{N}_c\mathbf{N}_c^{\mathrm{T}})^{-1}, \tag{2}$$

where $\mathbf{R}$ is measured spectral reflectances of training samples.

The PQR bases $\mathbf{V}$ are derived from principal component analysis (PCA)[15,16] on a set of spectral differences between the original spectra and the reconstructed spectra through the inverse transformation with $\mathbf{T}$ from $\mathbf{N}_c$. This spectral difference is expressed as:

$$\mathbf{E} = \mathbf{R} - \mathbf{T}\mathbf{N}_c. \tag{3}$$

Only the first three eigenvectors are preserved as the PRQ bases:

$$\mathbf{V} = (\mathbf{v}_1, \mathbf{v}_2, \mathbf{v}_3), \tag{4}$$

where $\mathbf{v}_i$ are eigenvectors in a set of the spectral difference.

Derhak and Rosen implemented the linear transformation between tristimulus vectors and spectral reflectance vectors, incorporating nonlinear combination of coordinates in the transformation.[4,6] For this implementation, the following vector $\mathbf{N}_c'$ is used instead of the tristimulus vector $\mathbf{N}_c$ in Eqs. (1)–(3):

$$\mathbf{N}_c' = \begin{bmatrix} X \\ Y \\ Z \\ XY \\ XZ \\ YZ \\ XYZ \end{bmatrix}, \tag{5}$$

where $[X, Y, Z]^{\mathrm{T}}$ are the tristimulus values $\mathbf{N}_c$. This modification with additional interaction is so-called 'XYZ+'. The computation routine on LabPQR is fully described in Ref. 6. Since Derhak and Rosen's implementation scheme was superior to the scheme without the 'XYZ+' in terms of the round-trip spectral reconstruction, the implementation scheme was utilized in this research.

In Derhak and Rosen's scheme, all the tristimulus values in the above calculations were normalized by tristimulus values of the white point of interest. However, from our experimental results, there was no significant difference between the schemes with or without the normalization in terms of the spectral reconstruction, thus no normalization for the tristimulus values was performed in this research.

Spectral Gamut

The first three dimensions of LabPQR are CIELAB. Those dimensions yield a traditional colorimetric gamut. The colorimetric response gamut in Figure 1 is an example of the gamut description that could be built from the first three dimensions of LabPQR. In addition to having a traditional colorimetric gamut, every point in the LabPQR colorimetric gamut is associated with a spectral gamut of PQR values that describe the metamer gamut for that colorimetric value.[5]

The printer represented has the PQR gamut shown in Fig. 1 for $(L^*, a^*, b^*) = (70, 50, 50)$. Each PQR value in this spectral gamut is associated with a metamer that has CIELAB colorimetry of $(70, 50, 50)$. Every other point in the CIELAB response gamut is associated with a different PQR gamut. For visualization purpose, the six-dimensional LabPQR gamut was divided into two three-dimensional encodings in Fig. 1.

Using the inexpensive linear calculation shown in Eq. (1), the original spectra that correspond to the given LabPQR values were reconstructed, as illustrated in Fig. 1. Note that each spectrum yields the identical CIELAB values, but different PQR values. The relationships between LabPQR and the spectral reconstruction are invertible.

Spectral Gamut Mapping

When attempting to produce a specific response from a color output device, one important consideration is determining if a request is outside the devices' rendering capability. The request is considered out-of-gamut when it is outside the palette of available responses. In color management, an out-of-gamut request must still be resolved to some response from the color output device. The set of rules used to guide this process when the request is a spectrum would be called spectral gamut mapping.

Described here is an approach to spectral gamut mapping. The spectral gamut mapping has two aspects: colorimetric and spectral. Rosen and Derhak proposed the spectral gamut mapping approach in which the two were performed independently.[5] In the colorimetric stage, one determined if a requested stimulus was within the colorimetric response gamut. If not, traditional colorimetric gamut mapping techniques were practiced to choose an in-gamut CIELAB. On the other hand, in the spectral stage, one determined if a requested spectrum was within the PQR spectral gamut for the in-gamut colorimetry. If not, spectral gamut mapping techniques were practiced to choose among valid device values. Rosen and Derhak's approach was reasonable, but two separated stages were necessary to recognize whether requested stimuli were within the colorimetric gamut and then if they were within the spectral gamut. Also,

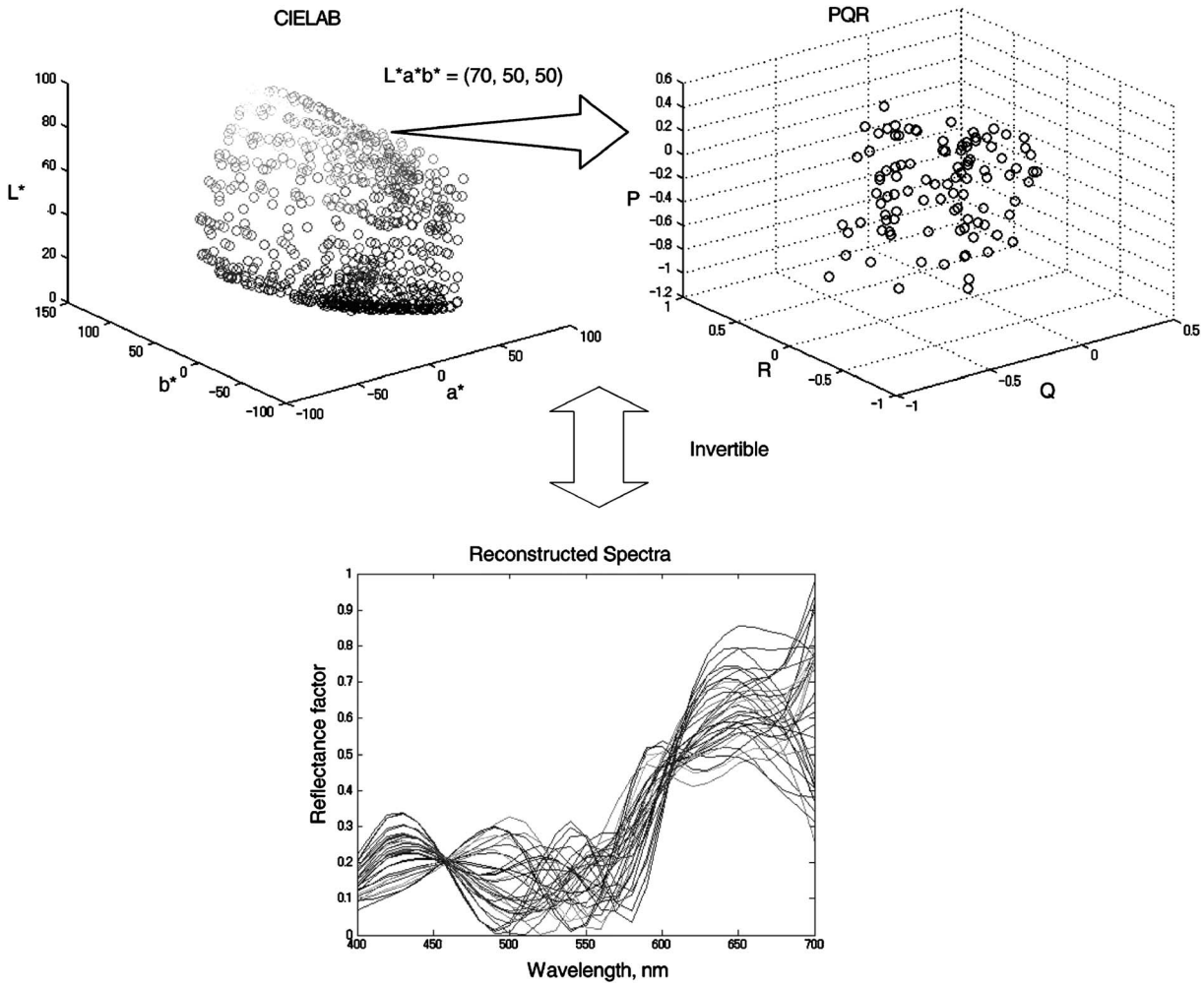

Figure 1. LabPQR colorimetric and spectral gamuts. Several different PQR combinations for $(L^*, a^*, b^*)=(70, 50, 50)$ are plotted in the PQR spectral gamut. The spectral reconstructions are derived from the LabPQR values.

the only consideration for the out-of-gamut CIELAB requests was to use standard colorimetric gamut mapping. No attempts were made to spectrally gamut map requests that were colorimetrically out-of-gamut.

Here, the colorimetric and spectral stages were combined and performed simultaneously. The full six-dimensional spectral gamut mapping was practiced in a single stage. Fractional area coverages of an ink jet printer for arbitrary requested spectra were computed by minimizing a single objective function: the weighted sum of CIEDE2000 color difference[17] and normalized Euclidian distance in PQR that yield the same range of spectral root-mean-square (RMS) error, defined as:

$$\text{ObjFunc1} = \text{Minimize}(\text{CIEDE2000} + k\Delta PQR), \quad (6)$$

where k is a weighting that may be empirically fitted.

Several studies have been reported on colorimetric gamut mapping techniques. Kato et al.[18,19] proposed three-dimensional gamut mapping approaches with the use of weighted color difference equations such as ΔE^*_{94}.[12] Since the weighted difference color equations including CIEDE2000 take into account a lack of uniformity and curvature of blue hue loci in CIELAB,[20,21] the three-dimensional approaches were effective in absolute colorimetric matching.[22] In the absolute colorimetric matching, the requested stimuli are mapped to nearest in-gamut stimuli, and no colorimetric change is caused if the requested stimuli are in-gamut $L^*a^*b^*$.

In a similar fashion, our proposed objective function for the spectral gamut mapping was defined. The first term on the right hand side of Eq. (6) implies the absolute colorimetric matching based on the CIEDE2000 color difference while the second term represents spectral matching to minimize the spectral error between requested and response stimuli. Equation (6) can be utilized globally regardless of whether the requested stimuli are within the colorimetric or spectral response gamuts. If the requested stimuli are within the colorimetric response gamut, as illustrated in Figure 2, the CIEDE2000 portion of Eq. (6) should vanish and the only active portion of the objective function will be the spectral RMS error. On the other hand, Eq. (6) will attend to both the colorimetric and spectral differences if the requested stimuli are outside the colorimetric gamut, as illustrated in Figure 3. Tuning the magnitude of k allows one to

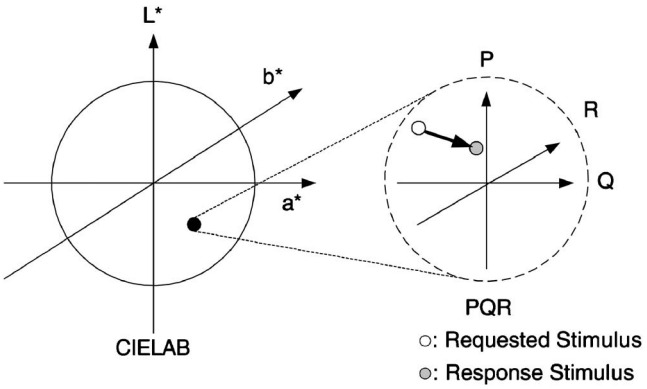

Figure 2. Spectral gamut mapping when the requested stimulus is within the colorimetric response gamut.

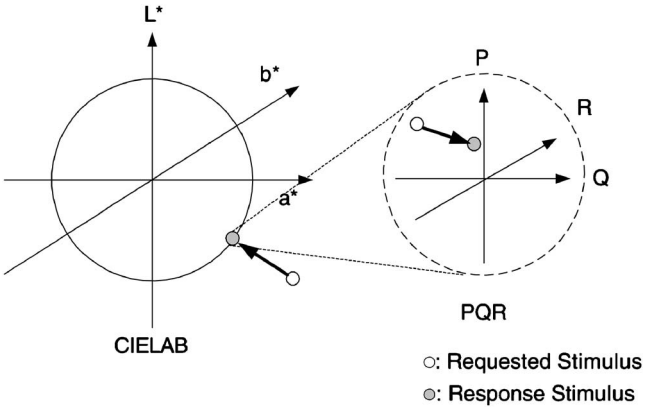

Figure 3. Spectral gamut mapping when the requested stimulus is outside the colorimetric response gamut.

choose an optimal trade-off between the colorimetric and spectral error. Choosing smaller values of k increases the relative importance of the colorimetric matching while larger values make the spectral aspect of the function more important.

Equation (6) is equivalent to minimizing spectral RMS error if the requested stimuli are within the colorimetric response gamut, because the Euclidian distance in PQR between a metameric pair is proportional to spectral RMS error. A proof is shown in the Appendix.

EXPERIMENTAL

A Canon i9900 dye-based ink jet printer with customized control driver was employed in this research. This printer had the capability of an eight-ink set, but only six were utilized: cyan (C), magenta (M), yellow (Y), black (K), red (R), and green (G). Since light cyan and magenta inks revealed spectral similarities, the light inks were not utilized. Spatial addressability of the ink jet printer was 1200×2400 dpi. All samples were printed on Canon Photo Paper Pro (PR-101) photo quality ink jet glossy paper. To have the print head of the ink jet printer stable while printing, neutral patches where the fractional area coverage of

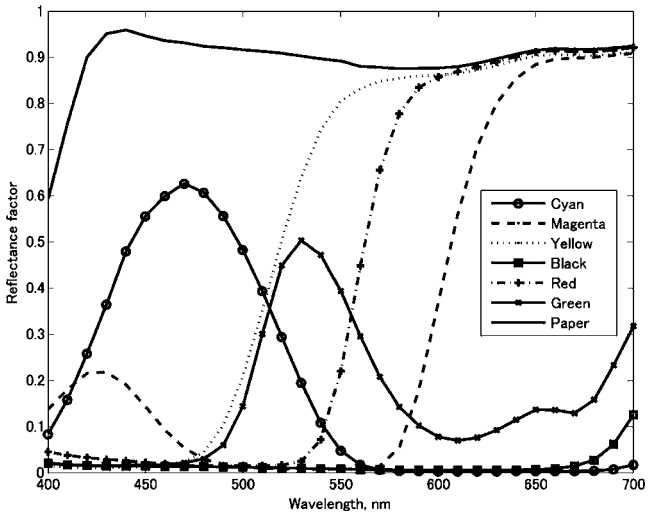

Figure 4. Spectral reflectance factor of each colorant at the maximum fractional area coverage and the paper substrate.

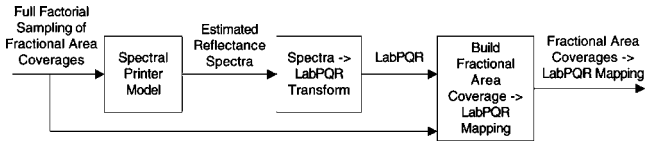

Figure 5. Schematic diagram for building the forward mapping from fractional area coverage to LabPQR.

each colorant was identical were printed between every target patch. A GretagMacbeth SpectroScan spectrophotometer was used for spectral measurements of the printed samples. The SpectroScan had a 4 mm aperture with a 45/0 annular geometry and measured spectral reflectance factor in the range between 380 and 730 nm in 10 nm intervals. To ensure consistency with previous research[4–6] only data between 400 and 700 nm were utilized. The measurement was carried out at least 12 hours after printing. Colorimetric values were calculated under illuminant D50 and for the CIE 1931 2° standard observer.

The spectral reflectance factor of each colorant at the maximum fractional area coverage was measured and plotted in Figure 4, along with spectral reflectance factor of the paper substrate. Since the ink jet printer was equipped with dye-based inks, unwanted long tail reflectance at longer wavelengths was observed for the C, K, and G inks. In particular, the long tail of the G ink was remarkable. The long tail is a typical spectral characteristic of dye-based inks.

In Figure 5, the steps for building the forward mapping from fractional area coverage to LabPQR are shown. This mapping associates a LabPQR value with every fractional area coverage value in a full factorial sampling of fractional area coverage space. First, the CMYKRG ink jet printer was spectrally characterized, in a similar fashion to Chen, Berns, and Taplin's approach.[1] For 729 print patches randomly distributed in the CIELAB space, this printer model achieved sufficient prediction accuracies: an average CIEDE2000 of

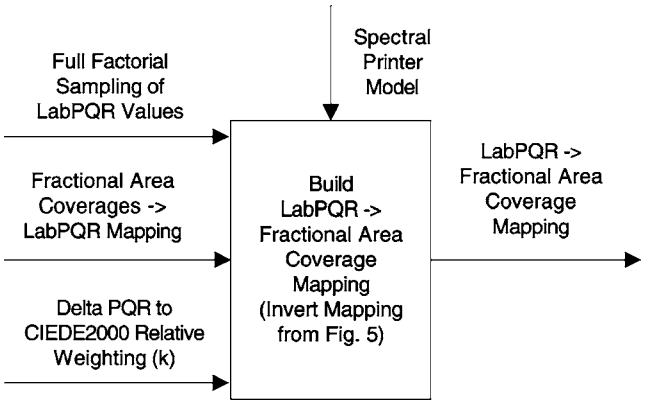

Figure 6. Schematic diagram describing inputs to the inversion process.

1.25 and average spectral RMS error of 0.63%. Second, using a set of the predicted spectra, spectra-to-LabPQR transform was built, following the mathematical procedure described above. In this stage, the reconstruction matrix **T** [Eq. (2)] and the PQR bases **V** [Eq. (4)] were determined prior to calculating the LabPQR values. Computationally, the corresponding CIELAB values were calculated from the tristimulus values. Finally, fractional area coverage to LabPQR mapping was performed, accounting for the relationship between the fractional area coverage and the LabPQR values of the input. For spectral color management, this mapping must be inverted because a specific set of the fractional area coverage values is required for any arbitrary spectrum, LabPQR in this case.

Figure 6 illustrates that the inversion relies on the spectral printer model and the choice of the weighting k in the objective function [Eq. (6)]. Within the inversion process of Fig. 6, a fractional area coverage value was chosen for each LabPQR such that the objective function was minimized for each. The MATLAB function in the Optimization Toolbox, *fmincon*, a constrained nonlinear optimization routine that uses a sequential quadratic programming method[14] was used as the optimization engine. The constraint here was that the fractional area coverage value of each colorant varied between 0 and 1, and the amount of the fractional area coverage values did not exceed the maximum ink limitation for the selected substrate.

RESULTS AND DISCUSSION

Building Spectra-to-LabPQR Transform

Using virtual spectral samples generated by the printer model, the reconstruction matrices **T** and **V** were derived with the 'XYZ+' method.[4–6] The training data set consisted of 729 samples randomly distributed in the CIELAB plus 6,620 samples uniformly spaced in fractional area coverages from 0 to 1 in five steps. This data set excluded samples of which fractional area coverages exceeded the maximum ink limitation for the selected substrate.

A set of the metameric blacks of the training data set, which were derived using Eq. (3), is plotted in Figure 7. There were relatively larger differences at longer wavelengths.

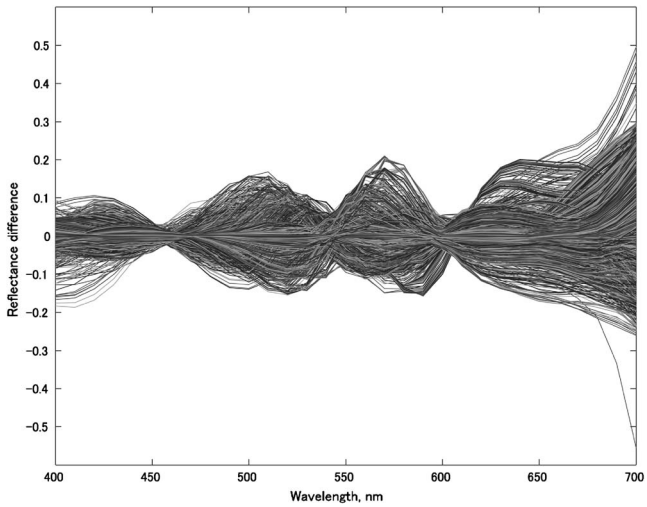

Figure 7. A set of the metameric blacks of the data set synthesized by the spectral printer model.

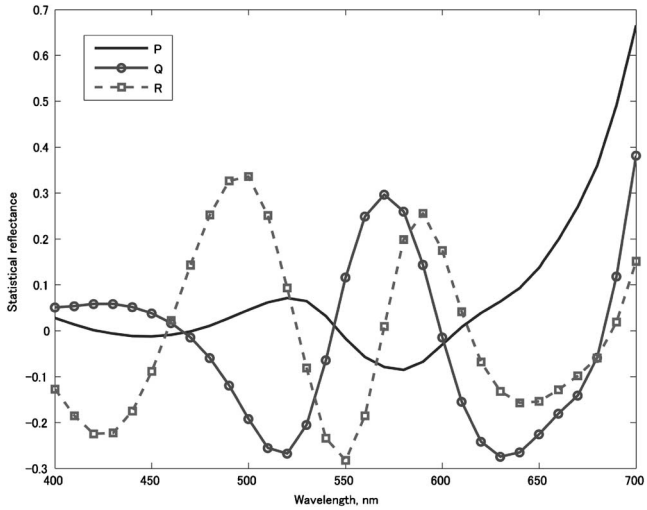

Figure 8. PQR vectors derived from PCA on the set of the metameric blacks of the training data set.

Maybe this is due to the long tail of the inks, as discussed in Fig. 4. Besides, the differences at wavelength of approximately 400, 500 and 570 nm were somewhat remarkable.

The PQR bases derived through PCA on the set of the metameric blacks are plotted in Figure 8. Each vector contained large statistical reflectance at longer wavelengths, accounting for the large spectral difference in this wavelength range, shown in Fig. 7. The P vector, the first eigenvector, had a relatively flat curve shape in comparison with the QR vectors, because the first eigenvector is considered to describe the general tendency of the sample set.[15,16] Also, the curve shapes tended to be less flat as the significance numbers of the eigenvectors increased.

Evaluating Round-Trip Spectral Reconstruction Accuracies Using the Spectra-to-LabPQR Transform

For evaluation of the round-trip spectral reconstruction accuracies, four different types of data sets were prepared:

Table I. Round trip accuracies of Virtual Prints, CC, CCDC, and Munsell in terms of spectral RMS error (%).

Data set	Virtual Prints	CC	CCDC	Munsell
Ave.	0.43	2.05	1.97	2.11
Max.	5.16	3.88	6.84	5.62
Std. Dev.	0.22	0.90	1.05	0.79
90th Percentile	0.62	3.63	2.97	3.06

1. A set of 805,355 patches synthesized by the spectral printer model, which were spaced in fractional area coverages in 11 steps (Virtual Prints)
2. GretagMacbeth ColorChecker (CC)
3. GretagMacbeth ColorChecker DC (CCDC)
4. Munsell Book of Color glossy edition containing 1600 patches[23] (Munsell)

In this evaluation, the LabPQR values of each data set were calculated using the spectra-to-LabPQR transform build from the training data set of the prints, and the spectra of each data set were reconstructed from the LabPQR values. Spectral differences between the original and the reconstructed spectra were calculated.

Table I summarizes the round-trip accuracies of each data set in terms of spectral RMS error. As expected, the reconstruction accuracies for Virtual Prints were superior to each other data set, but the reconstruction accuracies for the unknown data sets were acceptable, resulting in average spectral RMS errors of 0.43%, 2.05%, 1.97%, and 2.11% for Virtual Prints, CC, CCDC, and Munsell, respectively. As for the color difference, there was no difference within the round-trip, resulting in all the CIEDE2000 of 0.00. This clearly indicated that the spectra-to-LabPQR transform was sufficient for reconstructing the original spectra of any arbitrary inputs in terms of colorimetric matching.

The reconstructed spectral reflectances of the No. 1 and No. 15 patches of CC are plotted in Figure 9, along with the original spectra. The No. 1 patch indicated the second best reconstruction accuracy: spectral RMS error of 0.96% (The best was 0.43% for the No. 24 patch). The spectral reconstruction was excellent except at longer wavelengths. A lack of the reconstruction of CC at the longer wavelengths might be due to the long tail of the colorant. The No. 15 patch indicated the worst reconstruction accuracy: spectral RMS error of 3.76%. The curve shape of the reconstructed spectra was not smooth and negative reflectance factors were obtained in the range between 550 nm and 600 nm. Because the reconstructed spectra were generated in the six-dimensional LabPQR space, sharp curve changes of the original were not precisely reconstructed. Therefore, it was likely that the negative reflectance factors were computationally obtained where the spectral reflectance factors changed sharply. In this article, no clipping was performed if the reconstructed spectra included negative reflectance factor.

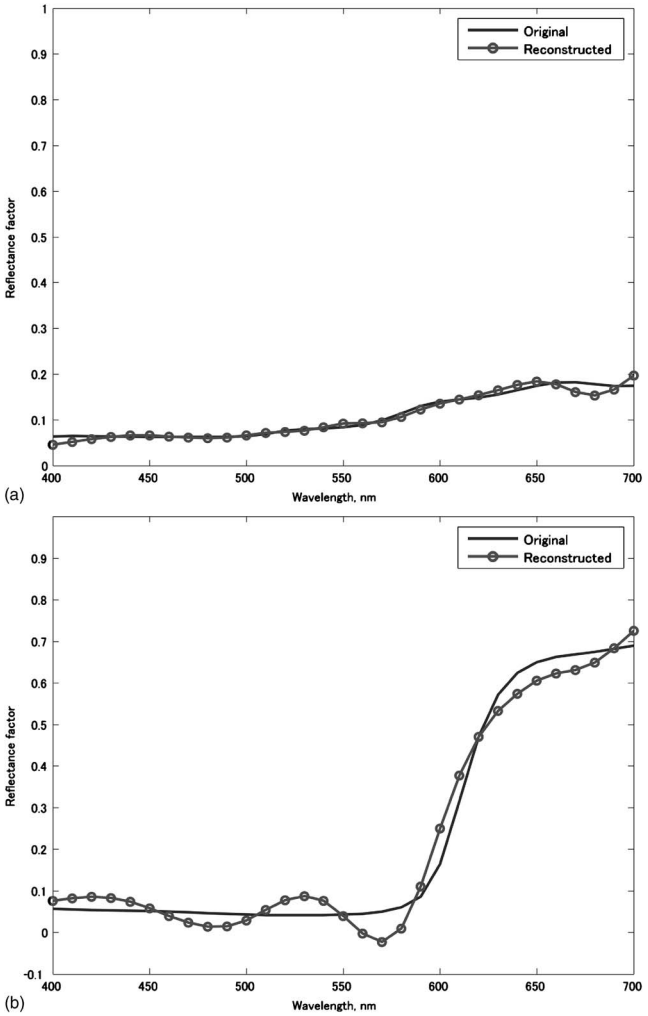

Figure 9. Comparison of spectral reflectance curves of the CC No. 1 (a) and No. 15 patches between the original and the reconstructed spectra through the round-trip.

Distributions of PQR Values

Using a set of 729 patches printed by the CMYKRG ink jet printer (Prints), which is randomly distributed in the CIELAB, the PQR values are plotted in the PQR space, shown in Figure 10. A large portion of the samples was centered $(P,Q,R)=(0,0,0)$. Besides, it was found in our experiment that dark colors tended to yield the PQR values close to $(0,0,0)$. Since the dark colors introduce lower spectral reflectance factors in flat curve shapes, the spectra of the dark colors might be easily reconstructed without using the PQR vectors. On the other hand, high chroma colors tend to locate on points far from the center of the PQR space. As mentioned above, every point LabPQR colorimetric gamut is associated with a different PQR gamut. Therefore, in practice, each PQR point in Fig. 10 belongs to each PQR gamut.

Figure 11 illustrates histograms of the PQR values of Prints and Munsell. As expected, the P values showed the larger distribution ranges, and the Q values showed the smaller distribution ranges. The order of these data sets corresponded to the significance of the eigenvectors, though Munsell was not utilized for building the spectra-to-LabPQR transform. Interestingly, the P values of Munsell were slightly shifted to the negative direction while the QR values were centered at approximately 0. Maybe this negative shift

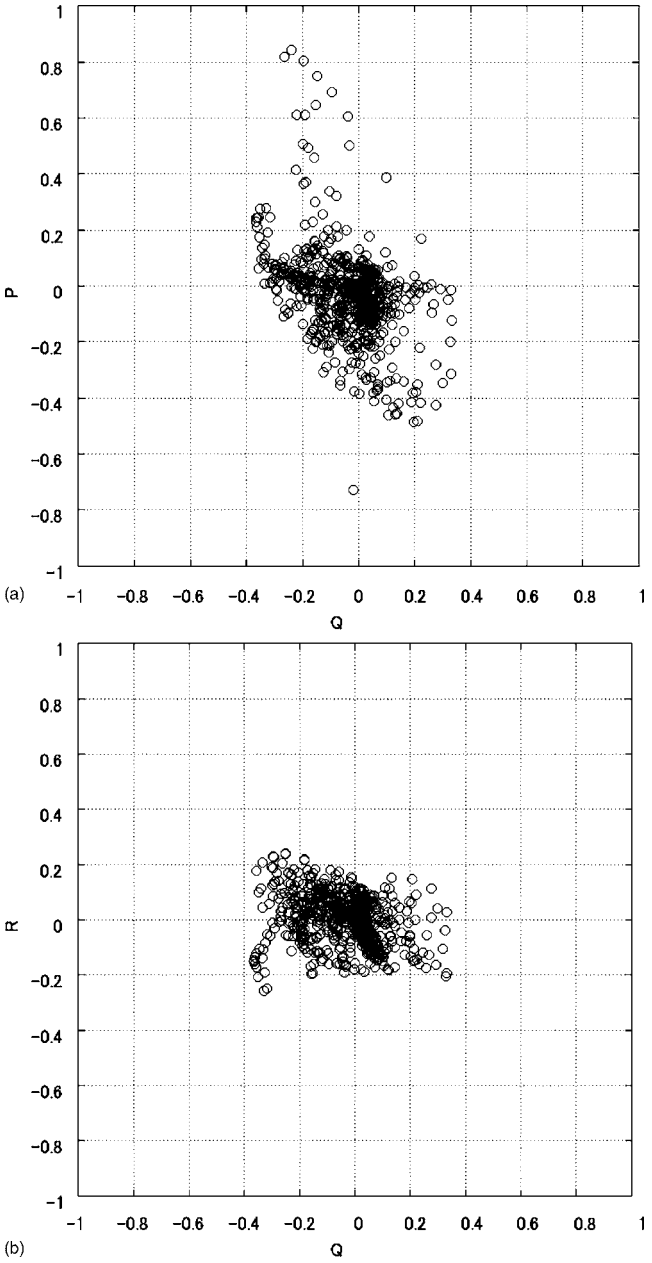

Figure 10. PQR values of Prints are plotted onto PQ (a) and QR coordinates.

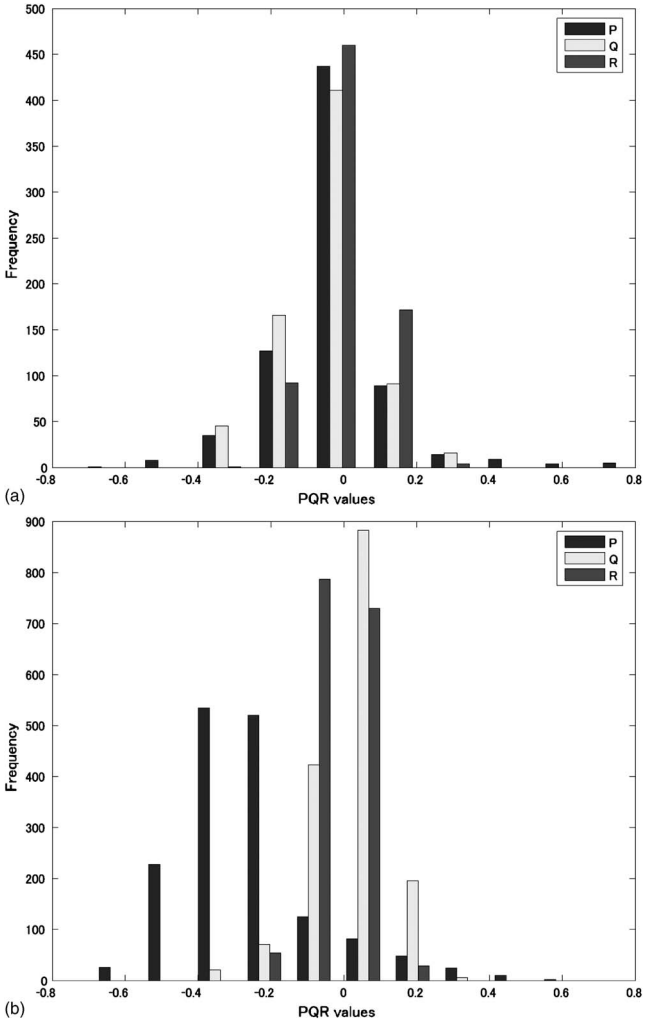

Figure 11. Histograms of the PQR values of Prints (a) and Munsell.

was due to higher reflectance of the P vector at longer wavelengths in Fig. 8. Since Munsell was made of paints and did not include many patches with the long tail, the P values tend to be negative values in order to reduce influences of the positive reflectance factors of the QR vectors in the same wavelength region.

The statistics of the PQR values of the verification data sets are summarized in Table II. For all the verification data sets, the ranges of the P values were approximately twice and three times as wide as the ranges of the Q and R values, respectively. That is, the P vector was the most significant basis for overall the data sets. The negative shifts of the P values were observed in CC and CCDC, as well as Munsell.

Finding an Optimal Weighting of the Objective Function

Our proposed spectral gamut mapping is performed using the objective function, shown in Eq. (6), so tuning of the weighting k is important in order to choose an optimal trade-off between the colorimetric and spectral difference. For finding the optimal k for Eq. (6), two different types of data sets were utilized: Prints, and 1,000 randomly selected feasible LabPQR values (Data set 1). Data set 1 was generated under a constraint that bounded reconstructed spectral reflectance factor between 0 and 1.

The spectral gamut mapping accuracies for Prints and Data set 1 are shown in Figures 12 and 13, respectively, indicating the trade-off between the colorimetric and spectral differences at different k values. It is clear from Fig. 12 that the spectral differences decrease with increasing k while the colorimetric differences increase. Data set 1 included 240 samples outside the colorimetric gamut of the printer, so the average colorimetric and spectral differences were larger than those of Prints. Interestingly, for k over approximately 200, the spectral RMS errors increase. Perhaps the reconstructed spectra have residual error and the colorimetric matching must, at some level, correct for that. From these results, it is reasonable to choose k between 20 and 50. In

Table II. Statistics of the PQR values of Prints, CC, CCDC, and Munsell.

	P values				Q values				R values			
	Ave.	Max.	Min.	Range	Ave.	Max.	Min.	Range	Ave.	Max.	Min.	Range
Prints	−0.028	0.843	−0.728	1.570	−0.043	0.337	−0.365	0.702	0.024	0.225	−0.259	0.484
CC	−0.211	0.357	−0.617	0.973	−0.019	0.192	−0.277	0.469	−0.037	0.078	−0.182	0.260
CCDC	−0.232	0.768	−0.792	1.560	−0.009	0.249	−0.351	0.600	−0.017	0.186	−0.326	0.512
Munsell	−0.258	0.665	−0.694	1.359	0.012	0.305	−0.362	0.667	−0.022	0.175	−0.266	0.441

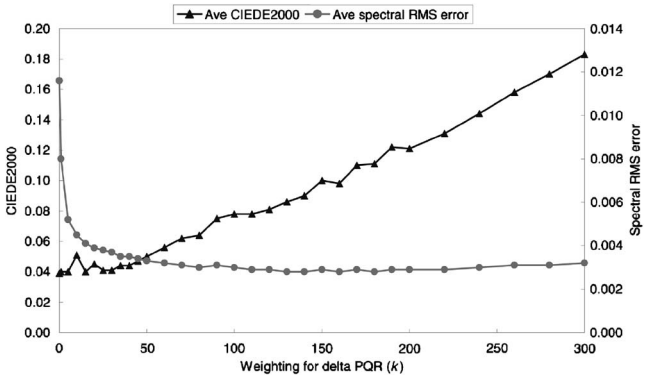

Figure 12. Spectral gamut mapping accuracies for 729 print patches (Prints) in a series of weighting (k).

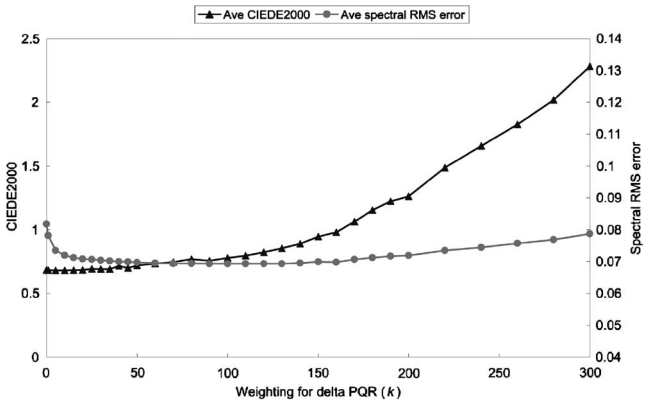

Figure 13. Spectral gamut mapping accuracies for 1000 randomly selected feasible LabPQR values (Dataset 1) in a series of weighting (k).

this article, k was set to 50, thereby attaching importance to spectral differences. The optimal weighting is likely data set dependent.

Feasibility of the Spectral Gamut Mapping

Using CC, CCDC, and Munsell, the feasibility of the proposed objective function [Eq. (6)] was explored in comparison to a full 31-dimensional approach and also a colorimetric-only mapping where the weighting k was set to zero. The full 31-dimensional and the colorimetric-only approaches are supposed to show the best accuracies in terms of spectral and colorimetric matchings, respectively. As mentioned in the Appendix, the Euclidian distance in PQR between a metameric pair is proportional to spectral RMS error, but not for a sample pair with different colorimetric values. To explore the efficiency of the six-dimensional LabPQR approach, the full 31-dimensional approach was also evaluated. The objective function minimized spectral differences in the full 31-dimensional reflectance space is expressed as:

$$\text{ObjFunc2} = \text{minimize}(\text{CIEDE2000} + k\ \text{sRMS}). \quad (7)$$

Tables III–V summarize the spectral gamut mapping performances for each data set. Since CCDC includes several samples exceeding the colorimetric gamut of the ink jet printer, its performance was worse. Colorimetrically, there was no significant difference between the approaches. Spectrally, the LabPQR and full spectral approaches were equivalent. For instance, the LabPQR approach resulted in an average CIEDE2000 of 0.03 and an average RMS error of 4.18% for CC. Because the CMYKRG ink jet printer cannot reproduce exact same curve shapes of CC, there still remained spectral differences. Consequently, the proposed approach with only six-dimensional LabPQR was able to yield an effective mapping for the CMYKRG ink jet printer in terms of both the colorimetric and spectral matchings.

Difference vectors in the CIELAB and PQR spaces are plotted in Figures 14 and 15, respectively, in which the tail of each arrow with a circle locates a requested stimulus and the head of each arrow locates a response stimulus. Figure 14 shows the difference vectors of CCDC in the CIELAB space. Obviously, there was no long arrow inside the printer's gamut while the closest CIELAB values on the gamut surface were chosen for the requested out-of-gamut stimuli. Thus, the colorimetric gamut mapping, one aspect of the spectral gamut mapping, was successfully performed using the proposed objective function. Figure 15 shows the difference vectors of CC in the PQR space. Since the PQR difference vectors of CCDC showed complicated configurations, CC was utilized instead. Most of the vectors moved toward the origin of PQR=(0,0,0) because the PQR values of the printer were concentrated around the origin, as previously discussed. Interestingly, the differences along the P axis were larger than those along QR bases; in contrast, the differences along the R axis were smaller. These relationships were in strong agreement with the significance order of the PQR vectors where the P vector was most significant and R vector was least significant. These results were reasonable because the ranges in P axis were larger than the ranges in other axes as mentioned in Fig. 11.

Table III. Spectral gamut mapping accuracies for CC in LabPQR, the full 31-dimensional reflectance space, and CIELAB color space.

	CIEDE2000 (D50, 2-degree)			Spectral RMS error (%)		
Color Space	LabPQR	Reflectance	CIELAB	LabPQR	Reflectance	CIELAB
Ave.	0.03	0.03	0.03	4.18	4.12	5.94
Max.	0.73	0.65	0.67	7.02	7.08	9.83
Std. Dev.	0.15	0.13	0.14	1.35	1.34	1.99
90th Percentile	0.00	0.00	0.00	6.07	6.03	8.01

Table IV. Spectral gamut mapping accuracies for CCDC in LabPQR, the full 31-dimensional reflectance space, and CIELAB color space.

	CIEDE2000 (D50, 2-degree)			Spectral RMS error (%)		
Color Space	LabPQR	Reflectance	CIELAB	LabPQR	Reflectance	CIELAB
Ave.	0.13	0.12	0.11	4.27	4.23	6.46
Max.	3.90	4.16	3.37	11.97	12.04	15.15
Std. Dev.	0.50	0.49	0.43	1.66	1.66	2.55
90th Percentile	0.01	0.00	0.00	6.07	5.94	10.05

Table V. Spectral gamut mapping accuracies for Munsell in LabPQR, the full 31-dimensional reflectance space, and CIELAB color space.

	CIEDE2000 (D50, 2-degree)			Spectral RMS error (%)		
Color Space	LabPQR	Reflectance	CIELAB	LabPQR	Reflectance	CIELAB
Ave.	0.02	0.02	0.02	4.54	4.51	6.73
Max.	2.17	2.10	2.02	10.61	10.58	15.61
Std. Dev.	0.15	0.14	0.13	1.36	1.37	2.25
90th Percentile	0.01	0.00	0.00	6.04	6.03	9.91

Two sets of the spectral reflectances of CC, which were reconstructed by using the spectral printer model with the fractional area coverages given from the spectral gamut mapping, are plotted in Figure 16 along with the original spectra. The No. 1 and No. 16 patches of CC showed representative results of the mapping approaches. There were no significant differences between spectral reflectance curves of the LabPQR and the full 31-dimensional approaches. Compared with the colorimetric-only approach, the improvements of the LabPQR approach at longer wavelengths and around the wavelength where the original curves change sharply were remarkable. Because our approach used the six-dimensional data, the reproductions are more flexible than the colorimetric-only approach. For the No. 1 patch, spectral RMS errors between the original and reproduced spectra of the LabPQR, full 31-dimensional, and colorimetric-only approaches were 3.29%, 3.27%, and 7.81%, respectively. For the No. 16 patch, the spectral RMS errors were 2.70%, 2.54%, and 4.12%, respectively. Since these two patches were within the colorimetric gamut of the printer and the results were derived by using the spectral printer model, there was no colorimetric errors between the original and the reproduction spectra of each approach.

Fractional Area Coverage Difference

As described in Fig. 6, inverting the forward mapping allows one to get a specific set of fractional area coverages of the printer for requested LabPQR values even if the requested LabPQR values are generated from print samples of the printer. In order to evaluate how efficiently the inversion was performed, the fractional area coverage differences between input and estimated fractional area coverages were calculated. For a six-color printer, the difference in a set of fractional area coverages is calculated as:

$$\text{Fractional Area Coverage Difference} = \sqrt{\sum_{i=1}^{6} (a_i - \hat{a}_i)^2/6}, \tag{8}$$

where a_i and $\hat{a}_i$ represent the fractional area coverages of the input and estimated ones derived by Eq. (6) at the optimal k of 50, respectively. The fractional area coverage varied between 0 and 1.

Using Prints, the fractional area coverage differences at k of 0 (colorimetric-only matching) and 50 were calculated and grayscale-coded into CIELAB plots are shown in

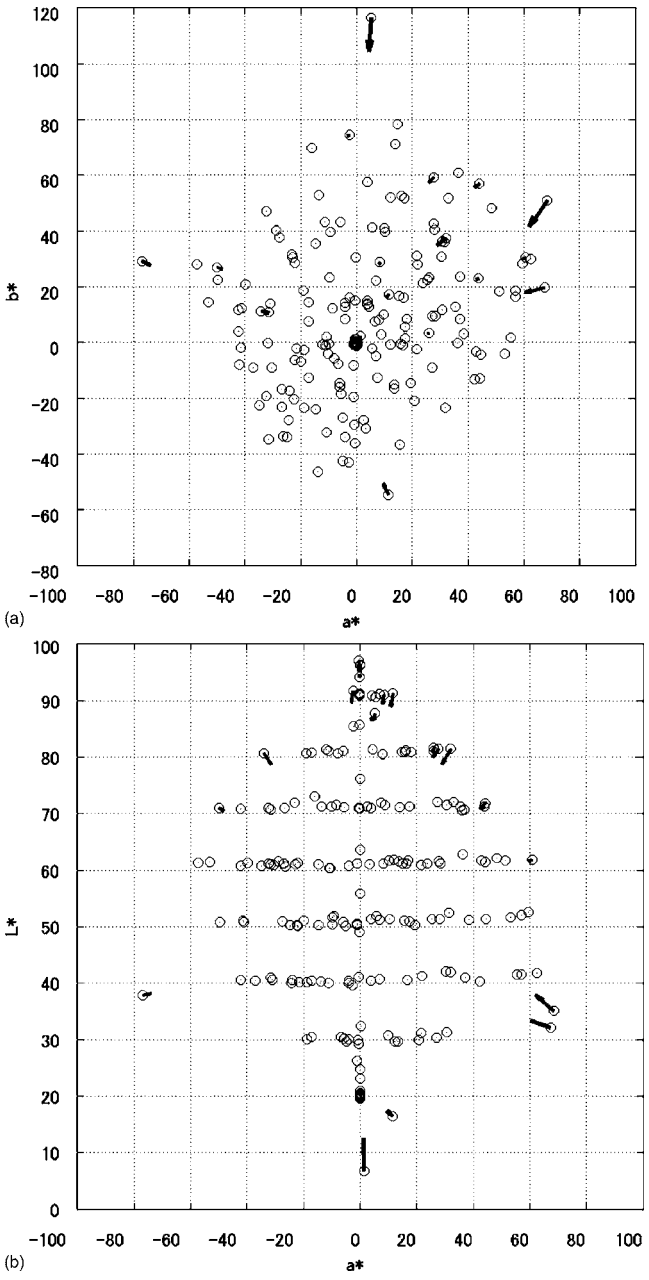

Figure 14. Difference vectors of CCDC in CIELAB are plotted onto a^*b^* (a) and L^*a^* coordinates. The tail of each arrow with a circle locates a requested stimulus and the head of each arrow locates a response stimulus.

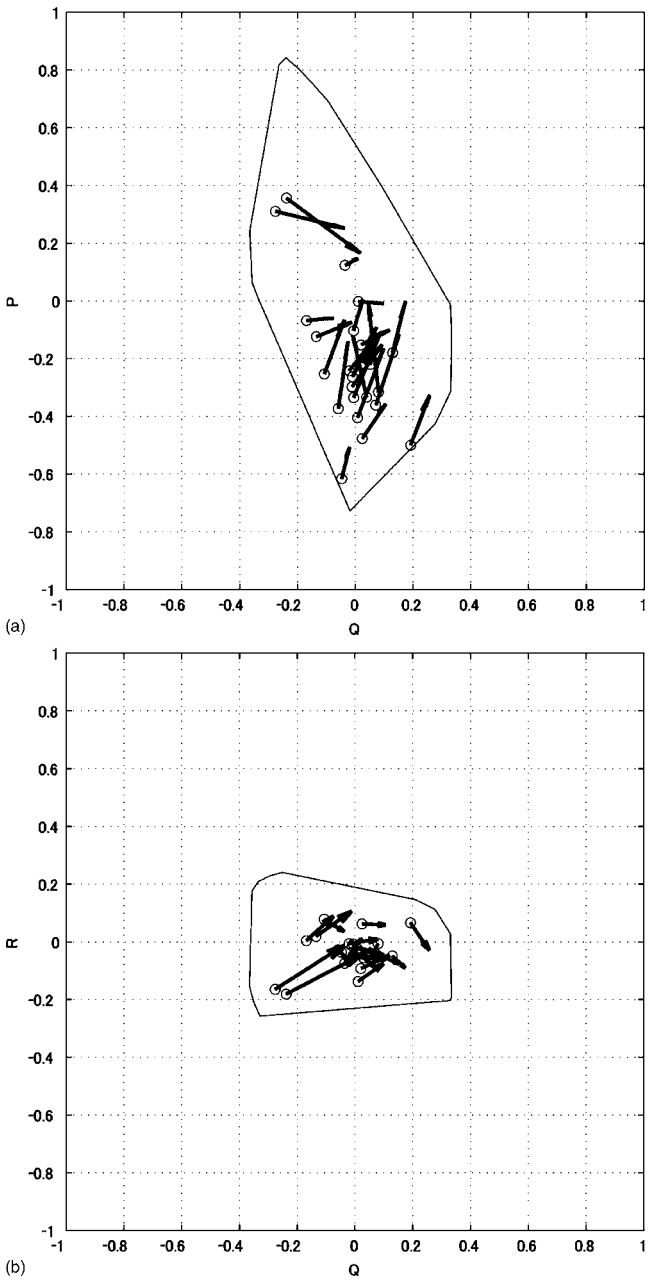

Figure 15. Difference vectors of CC in the PQR space are plotted onto PQ (a) and QR coordinates, along with the PQR gamut of the ink jet printer (solid lines). The tail of each arrow with a circle locates a requested stimulus and the head of each arrow locates a response stimulus.

Figure 17. For the results at k of 50, excellent estimation of the fractional area coverage was provided except at lower lightness and for red and green color regions. These areas of lower accuracy are not surprising. This is because the ink jet printer used in these experiments was equipped with green and red inks, likely leading to spectral redundancy[24,25] in those color regions. One thing to note is that there is no large difference around the boundaries of the colorimetric gamut. This indicates that few metameric pairs exist in those regions. The colorimetric-only approach ($k=0$) showed a similar behavior, but was worse than the LabPQR approach, resulting in average and maximum fractional area coverage differences of 11.12% and 61.69%, respectively, while the LabPQR approach indicated 7.43% and 43.97%, respectively. Therefore, spectral information might be useful to predict the input fractional area coverage of the printer when inverting the fractional area coverage to spectra relationship.

CONCLUSIONS

In this article, a spectral gamut mapping technique based on LabPQR has been explored using a six-colorant ink jet printer. LabPQR is a six-dimensional ICS where the first three dimensions are CIELAB values under a particular viewing condition, and the additional dimensions are spectral reconstruction dimensions describing a metameric black (PQR). First, spectra-to-LabPQR transform converting

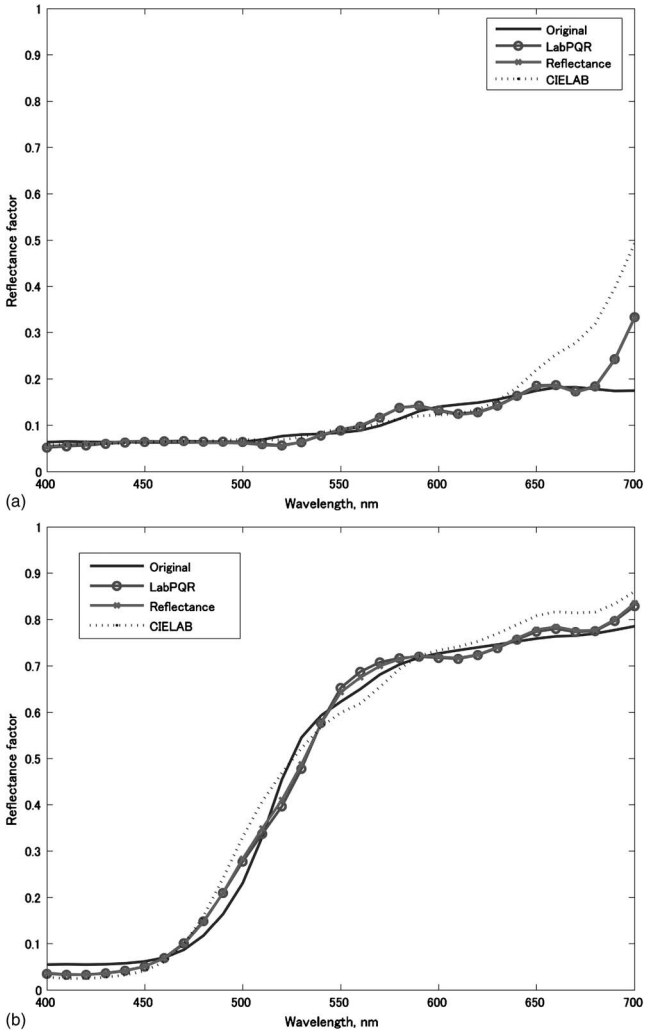

Figure 16. Comparisons of spectral reflectance curves of the CC No. 1 (a) and No. 16 patches between the spectra reproduced by three different mapping techniques: LabPQR, full 31-dimensional (Reflectance) and colorimetric-only (CIELAB) approaches. The original ones were also plotted.

LabPQR values from spectra was determined by using a spectral printer model. Second, the turning of parameters used in an objective function for the spectral gamut mapping was performed, accounting for a trade-off between colorimetric and spectral errors. Finally, feasibility of the proposed spectral gamut mapping approach for arbitrary LabPQR inputs was evaluated.

Using a data set generated by the spectral printer model, the spectra-to-LabPQR transform was successfully produced, resulting in sufficient reconstruction accuracies for the data set: an average CIEDE2000 of 0.00 and average spectral RMS error of 0.43%. Besides, the spectra-to-LabPQR transform was effective for reconstructing original spectra of the unknown data sets including the GretagMacbeth ColorChecker (CC). There was no colorimetric difference within round-trip including the spectra-to-LabPQR transform for any arbitrary inputs.

Through the computation above, it was found that the P basis, which was the most significant vector in the spectral coordinates, has yielded the largest distribution range for the unknown data sets, as well as the training data set used for building the spectra-to-LabPQR transform. The ranges of P values were approximately twice and three times as large as the ranges of Q and R values, respectively. The significance order of the PQR bases could be applied to the unknown data sets.

The spectral characterization of the CMYKRG ink jet printer has been inverted using the spectral gamut mapping technique based on LabPQR. The spectral gamut mapping was carried out with an objective function that minimized the weighted sum of CIEDE2000 and normalized Euclidian distance in PQR coordinate. This objective function was based on traditional absolute colorimetric matching techniques. Mathematically, the Euclidian distance in PQR between a metameric pair is proportional to spectral RMS error. This objective function can be utilized globally regardless of whether the requested stimuli are within the colorimetric or spectral response gamuts. At 1:50 weighting ratio k, CIEDE2000 to PQR difference, the proposed approach achieved the equivalent level of mapping accuracies to the full 31-dimensional approach. For CC, our approach resulted in an average RMS error of 4.18% with a maximum of 7.02%. In the spectral mapping, mapping directions in PQR led almost all stimuli toward the origin of PQR. Also, the differences along P axis between requested and response stimuli were the largest, in comparison with the differences in QR coordinates. As for the colorimetric matching, the proposed approach showed sufficient accuracies, resulting in an average CIEDE2000 of 0.03 with a maximum of 0.73 for CC. Thus, our proposed spectral gamut mapping has been a successful approach for both colorimetric and spectral matchings.

Following the spectral gamut mapping, fractional area coverage differences between input and estimated fractional area coverages were evaluated using print patches of the CMYKRG ink jet printer. From the evaluations overall CIELAB, it was found that the differences represented a unique set of fractional area coverage at the printer gamut. The larger fractional area coverage differences were obtained at lower lightness, and for red and green color regions while there was no large difference round the boundaries of the gamut.

There are a number of areas for future research. In this research, a spectra-to-LabPQR transform was generated using a specific data set, virtual spectral samples of CMYKRG ink jet printer, so the spectra-to-LabPQR transform has strong correlation with the data sets used for building it. Apparently, different spectra-to-LabPQR transforms will be provided if different types of printer or different types of targets are used. The reproduction accuracies might depend on the targets. Therefore, one of the new considerations of spectral color management would be how to generalize spectra-to-LabPQR transform that could be applied to different types of output devices. To do that, the transform may be generated using a number of sample collections. Also, the color-matching functions can be incorporated. The first term in Eq. (1) to reconstruct spectra from tristimulus val-

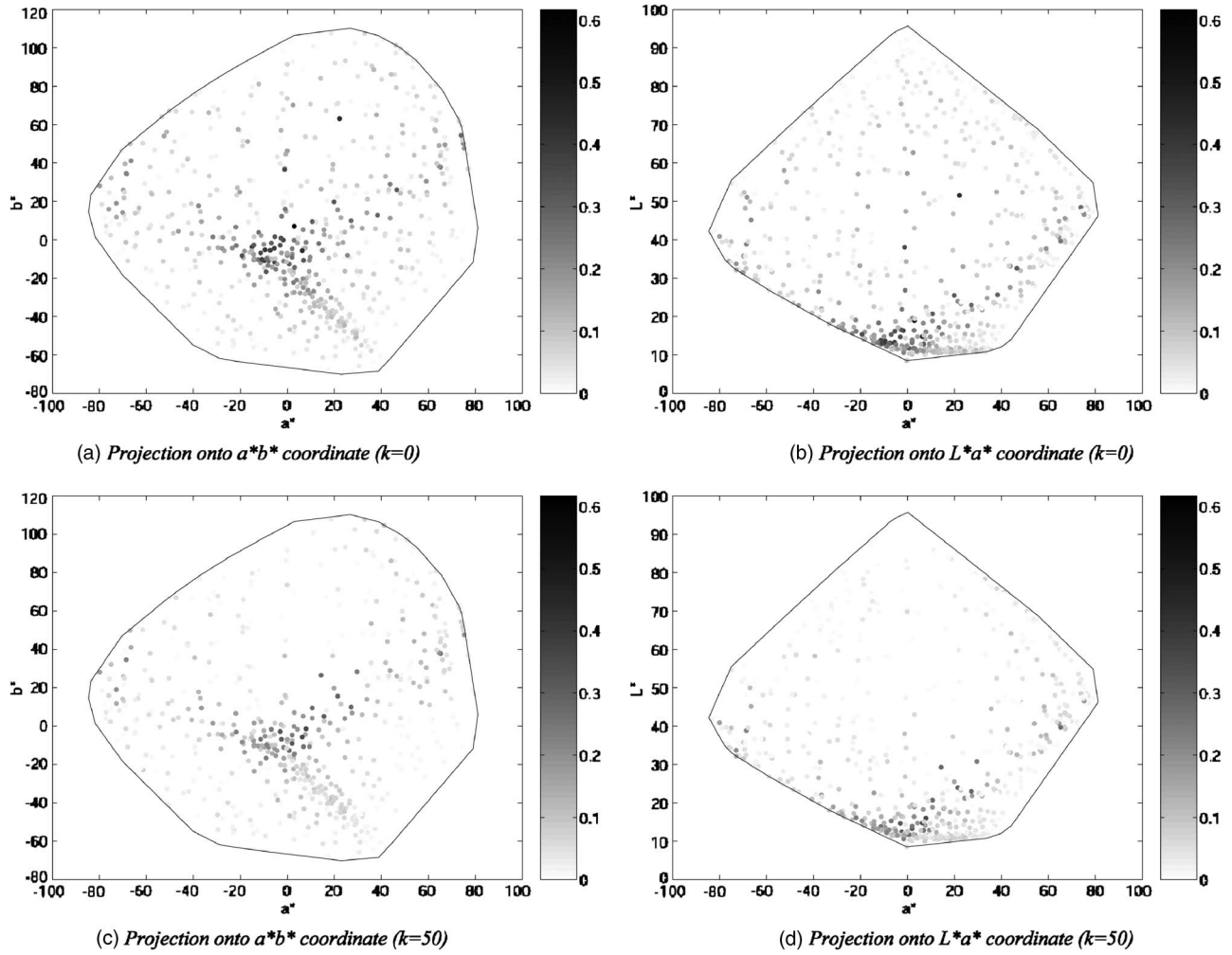

Figure 17. Fractional area coverage difference projected onto a^*b^* coordinate and onto L^*a^* coordinate at k of 0 (upper) and 50. The solid lines represent the colorimetric gamut boundaries of the printer.

ues may be derived using Cohen and Kappauf's spectral reproduction scheme know as the "matrix-R operation",[26] instead of using least square analysis on the sample collections.

Another consideration would be dimensionality of ICS. The goal of the present research is to build LUTs, so a low-dimensional ICS can be used to approximately match requested spectra to that which an output device is capable of delivering. However, since the loss of dimensionality could lead to spectral reconstruction inaccuracies, it is important to find the optimal trade-off between the reconstruction accuracy and the dimensionality of ICS.

The last is to produce LUTs based on LabPQR. Testing reproduction accuracies with the use of the LUTs would obviously be of interest. When attempting to produce the LUTs, the smaller memory size of the LUTs is desirable. However, the smaller size LUTs would certainly lead to lower reproduction accuracies. Exploring the trade-off between the size of the LUTs and reproduction accuracies would be another issue of spectral color management.

Acknowledgments
The authors would like to acknowledge Lawrence A. Taplin, Dr. Yongda Chen, and Dr. Noboru Ohta for their helpful suggestions. We would also like to acknowledge members of the Munsell Color Science Laboratory.

APPENDIX: PROOF ON PROPORTIONALITY OF EUCLIDIAN DISTANCE IN PQR TO SPECTRAL RMS ERROR

Equation (6) is equivalent to minimizing spectral RMS error if the requested stimuli are within the colorimetric response gamut, because the Euclidian distance in PQR between a metameric pair is proportional to spectral RMS error. To show this, let $\hat{\mathbf{R}}_1$ and $\hat{\mathbf{R}}_2$ denote reconstructed spectra of a metameric pair with the identical tristimulus values. From Eq. (1) we obtain

$$\hat{\mathbf{R}}_i = \mathbf{T}\mathbf{N}_c + \mathbf{V}\mathbf{N}_{p,i} \tag{9}$$

where

$$\mathbf{N}_{p,i} = \begin{bmatrix} p_i \\ q_i \\ r_i \end{bmatrix}. \tag{10}$$

The spectral RMS error between the reconstructed spectra is defined as

$$
\begin{aligned}
s\mathrm{RMS} &= \sqrt{(\hat{\mathbf{R}}_1 - \hat{\mathbf{R}}_2)^2/n} = \sqrt{(\mathbf{TN}_c + \mathbf{VN}_{p,1} - \mathbf{TN}_c - \mathbf{VN}_{p,2})^2/n} \\
&= \sqrt{\{\mathbf{V}(\mathbf{N}_{p,1} - \mathbf{N}_{p,2})\}^2/n} \\
&= \sqrt{\{(p_1 - p_2)\mathbf{v}_1 + (q_1 - q_2)\mathbf{v}_2 + (r_1 - r_2)\mathbf{v}_3\}^2/n}, \qquad (11)
\end{aligned}
$$

where n is the number of samples in a spectrum. Since $\|\mathbf{v}_i\| = 1$ and $\langle \mathbf{v}_i, \mathbf{v}_j \rangle = 0$ for $i \neq j$, Eq. (11) may be rewritten as

$$
\begin{aligned}
s\mathrm{RMS} &= \sqrt{\{(p_1 - p_2)^2 + (q_1 - q_2)^2 + (r_1 - r_2)^2\}/n} \\
&= \Delta PQR/\sqrt{n}. \qquad (12)
\end{aligned}
$$

Thus, Eq. (12) shows that the Euclidian distance of PQR is proportional to spectral RMS error for a metameric pair.

REFERENCES

[1] Y. Chen, R. S. Berns, and L. A. Taplin, "Six color printer characterization using an optimized cellular Yule-Nielsen spectral Neugebauer model", J. Imaging Sci. Technol. **48**, 519–528 (2004).

[2] D. R. Wyble and R. S. Berns, "A critical review of spectral models applied to binary color printing", Color Res. Appl. **25**, 4–15 (2000).

[3] L. A. Taplin and R. S. Berns, "Spectral color reproduction based on a six-color ink jet output system", *Proc. IS&T/SID Ninth Color Imaging Conference* (IS&T, Springfield, VA, 2001) pp. 209–213.

[4] M. W. Derhak and M. R. Rosen, "Spectral colorimetry using LabPQR - An interim connection space", *Proc. IS&T/SID 12th Color Imaging Conference* (IS&T, Springfield, VA, 2004) pp. 246–250.

[5] M. R. Rosen and M. W. Derhak, "Spectral gamuts and spectral gamut mapping", Proc. SPIE **6062**, 60620K (2006).

[6] M. W. Derhak and M. R. Rosen, "Spectral colorimetry using LabPQR - An interim connection space", J. Imaging Sci. Technol. **50**, 53–63 (2006).

[7] M. R. Rosen, F. H. Imai, X. Jiang, and N. Ohta, "Spectral reproduction from scene to hardcopy II: Image processing", Proc. SPIE **4300**, 33–41 (2001).

[8] M. R. Rosen, L. A. Taplin, F. H. Imai, R. S. Berns, and N. Ohta, "Answering Hunt's web shopping challenge: Spectral color management for a virtual swatch", *Proc. IS&T/SID Ninth Color Imaging Conference* (IS&T, Springfield, VA, 2001) pp. 267–273.

[9] M. R. Rosen, "Navigating the roadblocks to spectral color reproduction: data-efficient multi-channel imaging and spectral color management", Ph.D. Dissertation, (Rochester Institute of Technology, Rochester, NY, 2003).

[10] M. R. Rosen and N. Ohta, "Spectral color processing using an interim connection space", *Proc. IS&T/SID 11th Color Imaging Conference* (IS&T, Springfield, VA, 2003) pp. 187–192.

[11] G. Wyszecki and W. Stiles, *Color Science*, 2nd ed. (John Wiley and Sons, New York, 1982).

[12] R. S. Berns, *Billmeyer and Saltzman's Principles of Color Technology*, 3rd ed. (John Wiley and Sons, New York, 2000).

[13] S. Tsutsumi, M. R. Rosen, and R. S. Berns, "Spectral reproduction using LabPQR: Inverting the fractional-area-coverage-to-spectra relationship", *Proc. ICIS'06* (IS&T, Springfield, VA, 2006) pp. 107–110.

[14] E. K. P. Chong and S. H. Zak, *An Introduction to Optimization*, 2nd ed. (John Wiley and Sons, New York, 2001).

[15] R. A. Johnson and D. W. Wichern, *Applied Multivariate Statistical Analysis*, 5th ed. (Prentice Hall, Upper Saddle River, New Jersey, 2002).

[16] D. Y. Tzeng and R. S. Berns, "A review of principal component analysis and its application to color technology", Color Res. Appl. **30**, 84–98 (2005).

[17] M. R. Luo, G. Cui, and B. Rigg, "The development of the CIE 2000 colour-difference formula: CIEDE2000", Color Res. Appl. **26**, 340–350 (2001).

[18] N. Katoh, M. Ito, and S. Ohno, "Three-dimensional gamut mapping using various color difference formulae and color spaces", J. Electron. Imaging **8**, 365–379 (1999).

[19] N. Katoh and M. Ito, "Gamut mapping for computer generated images (II)", *Proc. IS&T/SID Fourth Color Imaging Conference* (IS&T, Springfield, VA, 1996) pp. 126–128.

[20] P. C. Hung and R. S. Berns, "Determination of constant hue loci for a CRT gamut and their predictions using color appearance spaces," Color Res. Appl. **20**, 285–295 (1995).

[21] F. Ebner and M. D. Fairchild, "Finding constant hue surfaces in color space", Proc. SPIE **3300**, 107–117 (1998).

[22] G. Sharma, *Digital Color Imaging Handbook* (CRC Press, Boca Raton, Florida, 2003).

[23] ~cs.joensuu.fi/~spectral/databases

[24] M. R. Rosen, E. F. Hattenberger, and N. Ohta, "Spectral redundancy in a six-ink ink jet printer", J. Imaging Sci. Technol. **48**, 192–202 (2004).

[25] E. F. Hattenberger, "Spectrally stable ink variability in a multi-primary printer", M.S. thesis (Rochester Institute of Technology, Rochester, NY, 2003).

[26] J. B. Cohen, "Color and color mixture: Scalar and vector fundamentals", Color Res. Appl. **13**, 5–39 (1988).